Testing the dynamical stability and the validity of the generalized second law within the phantom dynamical dark energy model

Naseeba K. M.*
Department of Physics, Government Brennen College, Dharmadam, Thalassery 670106, India

Sarath Nelleri† and Navaneeth Poonthottathil‡
Department of Physics, Indian Institute of Technology, Kanpur 208016, India

(Received 13 August 2023; accepted 28 February 2024; published 18 March 2024)

Hubble constant (H_0) tension and tension in the matter fluctuation amplitude (s_8) are fascinating puzzles in cosmology nowadays. The phantom dynamical dark energy model (PDDE), also known as the little sibling of the big rip, is an abrupt event that can happen in the far future evolution of the universe. A recent analysis of the PDDE model based on cosmic microwave backround radiation data shows that the model is a potential candidate to alleviate these tension problems. In this work, we study the background evolution of the universe within the PDDE model. Analysis based on the SNIa + BAO + OHD data shows that the model successfully explains the late-phase acceleration of the universe. Also, the values of the cosmological parameters computed by the PDDE model are consistent with those obtained by the ΛCDM model for the same dataset. However, most of the phantom dark energy models do not give a stable solution in the asymptotic future. In this regard, we address the PDDE model's dynamical stability and test the validity of the generalized second law (GSL) of thermodynamics. We show that the model is dynamically unstable and violates the GSL. The model does not satisfy the convexity condition, so the universe does not behave as an ordinary macroscopic system within the PDDE model.

DOI: 10.1103/PhysRevD.109.063528

I. INTRODUCTION

Various cosmological observations revealed that the present expansion of the universe is accelerating [1–9]. The ΛCDM model is the simplest model that explains the observed acceleration [10,11]. However, the concordance ΛCDM model faces the difficulties such as fine-tuning [12], cosmic coincidence [13], and tension observed in the cosmological parameters computed using the lower [14–16] and higher [3] redshift datasets. Numerous alternate cosmological models have been proposed to tackle these issues and explain the late-phase acceleration. Some of these models modify the curvature term in the Einstein field equation known as modified gravity models (see Refs. [17–21]). Other favorites include models that modify the energy-momentum tensor of the field equations known as modified dark energy models [22–40].

The phantom dynamical dark energy model (PDDE) that smoothed the big rip singularity was presented in Ref. [41]. In this model, the Hubble parameter and the scale factor diverge, but the first derivative of the Hubble parameter does not blow up and hence the name, little sibling of the big rip; the event happens at an infinite cosmic time. In addition, the model was studied by Bouali *et al.*, who put constraints on the model parameters, which are consistent with the observation [42]. Further extension of this model, including the interaction, is presented in Ref. [43]. These models are found to be as competent as the ΛCDM to explain the evolution of the universe at the background level. Recently, Dahmani *et al.* [44] studied the PDDE model extensively using the latest observational probes such as the cosmic microwave backround radiation (CMBR) [3], Type Ia supernovae (SNe Ia) [45], and baryon acoustic oscillation (BAO) datasets, which showed that the model is successful in alleviating the tension problems in cosmology.

While the success of phantom dark energy models explains the accelerated expansion of the universe, certain models in this category exhibit dynamical instability. The dynamics of phantom cosmologies are presented in [46–49]. The phantom dark energy exerts a negative pressure with an equation of state parameter less than -1. Such values of the equation of state parameter require the violation of dominant energy condition $(p + \rho) < 0$. The violation of the dominant energy condition leads to the instability of the system since the satisfaction of the dominant energy condition is a sufficient condition of the Hawking-Ellis conservation theorem [50,51]. Physically, this conservation theorem ensures the stability of the classical vacuum. Hence, for

*nasikm2001@gmail.com
†sarathn@iitk.ac.in
‡navaneeth@iitk.ac.in

phantom dark energy models one cannot guarantee the stability of the vacuum on the classical level. For instance, the dynamical stability analysis of the phenomenological emergent dark energy model was performed in [49]. The analysis based on the dark energy sound speed showed that the phantom dark energy dominated epoch is unstable. In addition, the authors of Ref. [46] considered a specific toy model where a phantom oscillator is coupled to an ordinary oscillator where the model violates the null dominant energy condition, and hence, the resulting spacetime is stable to a small linear perturbation while it is unstable under the higher order effects. Furthermore, investigation of the phase space dynamics of a universe filled with bulk viscous matter, radiation, and phantom dark energy showed that viscous phantom solutions with a stable behavior are not allowed [52]. However, phantom models with stable late-time solutions also exist and are discussed in [53–55]. The phase space analysis of phantom cosmological models with interacting dark sectors presented in [53,54] lead to stable late-time solutions corresponding to an accelerating universe. The phase space portrait of the homogeneous and isotropic universe by taking different coupling functions between dark energy models and bulk viscous dark matter is shown in [55]. The critical points and respective eigenvalues for different dynamical quantities shows the existence of a dynamically stable universe. These studies show that one cannot guarantee a stable universe within phantom dark energy models. Consequently, the primary objective of this study lies in testing the dynamical stability of the PDDE model.

The method of dynamical systems is a widely used set of tools in cosmology to check the asymptotic stability of a cosmological model [56,57]. The stability of the critical points is examined using the linear stability theorem [58]. The existence of a future attractor solution can also be investigated by analyzing the phase space plot. However, both the phase space and stability analysis fail to provide information on the stability of the critical point when it is nonhyperbolic [59,60]. In such a case, the center manifold theory helps us to understand the system's behavior by reducing the dimensionality of the system near that nonhyperbolic point [58,61]. In the PDDE model, one of the critical points is nonhyperbolic; hence, we use the center manifold theory to examine the stability of the model at that point. Our analysis shows that the PDDE model has no stable fixed point either in the matter dominated or in the late accelerating phase.

There exist several studies in the literature focused on the thermodynamics of the expanding universe [62–67]. We perform thermodynamic analysis similar to the thermodynamics of a black hole by treating the universe as a closed system [68,69]. Bekenstein and Hawking showed that the entropy of black holes is directly proportional to the area of their event horizon [70–72]. They also showed that black holes satisfy the generalized second law [71]. It states that the sum of the entropy of ordinary matter outside the black hole and one quarter of the area of the black hole's event horizon can never decrease with time [62]. Black hole thermodynamics can be extended to cosmology by considering the universe as an isolated thermodynamic system filled with a cosmic fluid and bounded by some horizon [68]. In cosmological framework, the apparent horizon is mostly used instead of the event horizon since the apparent horizon is a physically significant thermodynamic surface [68]. As far as the apparent horizon is considered as the universe's radius, the generalized second law of thermodynamics is always generally valid [73]. We analyze the validity of the generalized second law of thermodynamics within the PDDE model.

The paper is structured as follows. In Sec. II, we present the phantom dynamical dark energy model. In Sec. III, we constrain the model parameters using observational data and discuss the significance of each parameter and its cosmological implications. In Sec. IV, we study the evolution of cosmographic parameters. In Sec. V, we perform the dynamical system analysis to test the dynamical stability of the PDDE model. Further, we study the entropy evolution and validity of the generalized second law of thermodynamics (GSL) in Sec. VI. Finally, we summarize the conclusions of the work in Sec. VII.

II. THE PDDE MODEL

In the standard model of cosmology, we have the cosmological constant with the equation of state $\omega_\Lambda = -1$. Hence, the dark energy density ρ_Λ and the corresponding pressure satisfy the equation $\rho_\Lambda + p_\Lambda = 0$. In the PDDE model the phantom dark energy density ρ_D and the corresponding pressure p_D satisfies the equation

$$\rho_D + p_D = -\frac{\alpha}{3}, \tag{1}$$

where ρ_D has a specific form given by

$$\rho_D(z) = \rho_{D_0} - \alpha \ln(1+z), \tag{2}$$

where z is the redshift and ρ_{D_0} is the dark energy density at present [41]. The α is assumed to be a positive constant, and its nonzero value distinguishes this model from the standard ΛCDM model. Obtaining the equation of state parameter ω_D from Eqs. (1) and (2) is straightforward:

$$\omega_D = -\left(1 + \frac{\alpha}{3(\rho_{D_0} - \alpha \ln(1+z))}\right). \tag{3}$$

It is evident from Eq. (3) that the present model mimics quintessence behavior of dark energy ($\omega_D > -1$) for $\alpha < 0$ and reduces to the ΛCDM model when $\alpha = 0$. In the following discussion, we focus on the case $\alpha > 0$, for which the model shows a phantom behavior ($\omega_D < -1$). The nonrelativistic matter is assumed to have its kinetic pressure zero, and it satisfies the conservation equation

$$\dot{\rho_m} + 3H\rho_m = 0, \tag{4}$$

where the overdot represents the derivative with respect to cosmic time, which on solving gives $\rho_m = \rho_{m_0}(1+z)^3$. In this work, we mainly focus on the late-phase cosmology. Hence, we avoid the radiation density as its current value is negligibly small compared to dark matter and dark energy densities. Also, the latest CMBR data obtained by the Planck Collaboration suggest that spatial curvature is consistent with a flat universe [3]. With these observational constraints, the first Friedmann equation takes the form

$$H^2(z) = H_0^2(\Omega_{m_0}(1+z)^3 + \Omega_{D_0} - \Omega_{\text{pdde}}\ln(1+z)), \tag{5}$$

where H_0 is the Hubble parameter at present, $\Omega_{m_0} = 8\pi G\rho_{m_0}/3H_0^2$ is the present value matter density parameter, $\Omega_{D_0} = 8\pi G\rho_{D_0}/3H_0^2$ is the dark energy density parameter, and $\Omega_{\text{pdde}} = 8\pi G\alpha/3H_0^2$ is the parameter that signifies the PDDE model. From Eq. (5), when $z = 0, H = H_0$, where H_0 is the Hubble parameter at present. In the extreme past, $z \to \infty (1+z)^3$ dominated over the $\ln(1+z)$, and hence it is conclusive that the non-relativistic matter dominated over the dark energy in the past. In the far future, when $z \to -1$, matter density tends to zero, and dark energy density tends to infinity. Hence, the Hubble rate diverges in this limit while $\dot{H}$ is a finite constant.

III. OBSERVATIONAL CONSTRAINTS ON MODEL PARAMETERS

The PDDE model has three independent free parameters H_0, Ω_{m_0}, and Ω_{pdde}. The Ω_{D_0} and Ω_{m_0} satisfy the equation $\Omega_{m_0} + \Omega_{D_0} = 1$. Our next aim is to constrain these parameters by confronting the model with the observational data. We adopt the Markov chain Monte Carlo (MCMC) method for the parameter inference [74]. In this work, we mainly focus on the late-phase cosmology, and hence, we use cosmological data obtained at low redshift. The dataset comprises Type Ia supernovae data taken from the pantheon sample [45], BAO data [75–78], and observational Hubble data (OHD) [79]. The fundamental input for calculating the marginal likelihood of the model parameters is the prior range for each model parameter. We use a uniform prior following Ref. [44] for all the parameters. The pantheon sample consists of 1048 redshift (z) vs apparent magnitude (m) of Type Ia supernovae in the redshift span $0.01 \leq z \leq 2.3$ [45]. To obtain the apparent magnitude from the theory, we use the following expression:

$$m(z) = 5\log_{10}\left[\frac{d_L(z)}{\text{Mpc}}\right] + M + 25. \tag{6}$$

Here, M is the absolute magnitude of the Type Ia supernovae, and d_L is the luminosity distance that can be related to the expansion rate $H(z)$ as

$$d_L(z) = c(1+z)\int_0^z \frac{dz'}{H(z')}, \tag{7}$$

where c is the speed of light in vacuum expressed in km/s. The χ^2 for the SNe Ia data is computed using the expression

$$\chi^2_{\text{SNIa}} = \sum_{i=1}^{1048} \frac{[m_{\text{th}}(z_i, H_0, \Omega_{m_0}, \Omega_{\text{pdde}}, M) - m_{\text{obs}}(z_i)]^2}{\sigma(z_i)^2}, \tag{8}$$

where m_{th} and m_{obs} are the apparent magnitude computed using the PDDE model and one obtained by observation, respectively, and σ is the corresponding error in the measurement. The BAO measurements include the transverse comoving distance, which is equal to the line of sight comoving distance for flat space and is expressed as [80]

$$D_M(z) = D_c(z) = \frac{c}{H_0}\int_0^z \frac{dz'}{h(z')}, \tag{9}$$

and the volume averaged angular diameter distance

$$D_V(z) = \left[\frac{cz}{H_0}\frac{D_M^2(z)}{h(z)}\right]^{1/3}. \tag{10}$$

We use BAO data presented in Ref. [80] for the analysis. The χ^2 for the BAO data is obtained using the expression

$$\chi^2_{\text{BAO}} = \sum_{i=1}^{N} \frac{[A_{\text{th}}(z_i, H_0, \Omega_{m_0}, \Omega_{\text{pdde}}) - A_{\text{obs}}(z_i)]^2}{\sigma(z_i)^2}, \tag{11}$$

where A_{th} and A_{obs} are the theoretical and observed values of the physical quantity [$D_M(z_i)$ or $D_V(z_i)$] obtained from the BAO data, respectively, and N is the number of data points in the BAO measurement. The chi-square degrees of freedom ($\chi^2_{\text{d.o.f}}$) is defined as $\chi^2_{\text{min}}/(n-k)$, where k is the number of parameters of the model and n is the total number of data points [81,82]. The OHD dataset contains 43 redshifts versus Hubble parameter data in the redshift range $0.07 \leq z \leq 2.36$ [80,83]. This dataset includes the Hubble parameter obtained from cosmic chronometers, radial BAO signals in the distribution of galaxies and BAO signals in the Lyman α forest distribution. The χ^2 for the OHD data can be computed using the expression

$$\chi^2_{\text{OHD}} = \sum_{i=1}^{43} \frac{[H_{\text{th}}(z_i, H_0, \Omega_{m_0}, \Omega_{\text{pdde}}) - H_{\text{obs}}(z_i)]^2}{\sigma(z_i)^2}, \tag{12}$$

where H_{th} and H_{obs} are the Hubble parameter computed theoretically using the PDDE model and the corresponding observed one, respectively. Then the total χ^2 is of the form

$$\chi^2_{\text{total}} = \chi^2_{\text{SNIa}} + \chi^2_{\text{BAO}} + \chi^2_{\text{OHD}}. \tag{13}$$

The parameter set (H_0, Ω_{m_0}, Ω_{pdde}, M) that minimizes the $\chi^2_{\text{total}} = -2\ln\mathcal{L}$, where $\mathcal{L}$ is the likelihood, is considered as

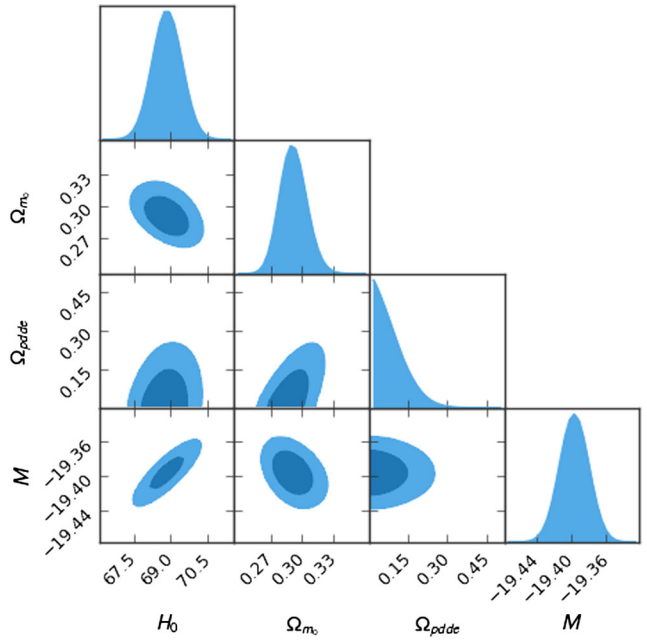

FIG. 1. The 2D confidence contour for 68% and 95% probabilities and 1D posterior distribution of the model parameters using the SNIa + BAO + OHD dataset. The prior ranges chosen for model parameters are $40 \leq H_0 \leq 100$, $0 \leq \Omega_{m_0} \leq 1$, $0 \leq \Omega_{\rm pdde} \leq 1$, and $-20 \leq M \leq -18$.

the best-fit parameters. We employed a stable, well tested, and open source PYTHON implementation of the affine invariant ensemble sampler for the MCMC, developed by Goodman and Weare to perform parameter inference. We also used the multiprocessing module from the PYTHON standard library to reduce the computation time. For further details regarding the emcee and its implementation see Ref. [84]. The best-fit model parameters are presented in Table I. For the SNIa + BAO + OHD dataset, the marginal likelihood of the model parameters is shown in Fig. 1. The minimum χ^2 obtained is 1064.54 with $\chi^2_{\rm d.o.f} = 0.974$. From Table I, it is clear that the estimated values of H_0, Ω_{m_0}, and M are consistent with the standard values obtained in the literature [2,3]. The phantom dark energy density $\Omega_{\rm pdde}$ that characterizes the PDDE model is 1 order of magnitude less than the matter density as expected. We do not expect much deviation from the ΛCDM predictions. Also, the large value of the standard deviation, which is comparable to the best-fit value, indicates that the significance of the nonzero value of $\Omega_{\rm pdde}$ is $\sim 1\sigma$, which is statistically less significant. At this juncture, it is important to compare our results with the results obtained in Ref. [44]. In Ref. [44], the authors estimated the parameters of the PDDE model using three different data combinations Planck18, Planck18 + BAO, and Planck18 + BAO + Pantheon. The primary focus of their study was centered around the investigation of the Hubble tension problem within the PDDE framework. Hence, they used CMBR data along with the low redshift datasets. The main results from their analysis is that the PDDE model can alleviate the H_0 and S_8 tensions to 3σ and 2.6σ, respectively. On the other hand, our analysis is mainly focus on the thermodynamic and dynamic stability of the model. Hence, we estimated the model parameters using low redshift data since we are interested in the far future stability of the model. The difference in the cosmological data taken for the parameter estimation leads to the observed discrepancies between their best-fit results with the present study. However, the parameter values we found in our analysis are very similar to the values they found in their study, which included Type Ia supernovae data.

TABLE I. The best-fit model parameters of the PDDE model and its uncertainties within the 1σ confidence limit.

Data	SNIa + BAO + OHD
H_0	68.86 ± 0.5746
Ω_{m_0}	0.291 ± 0.011
$\Omega_{\rm pdde}$	0.063 ± 0.059
M	-19.39 ± 0.0157

IV. EVOLUTION OF COSMOGRAPHIC PARAMETERS

In this section, we examine the evolution of various cosmographic parameters to understand how well the PDDE model explains the background evolution of the universe. The parameter of fundamental importance in cosmology is the Hubble parameter. The equation for the Hubble parameter is presented in Eq. (5) and its evolution against the redshift is depicted in Fig. 2. The evolution of the Hubble parameter in the PDDE model is almost similar to the ΛCDM model in the past and at

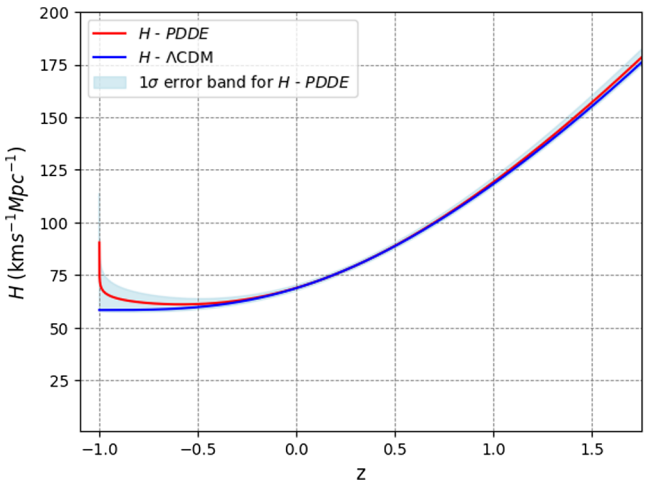

FIG. 2. The evolution of Hubble parameter (H) with redshift (z) is plotted for the PDDE model with error band and ΛCDM using the best-fit model parameters obtained for the SNIa + BAO + OHD data combination.

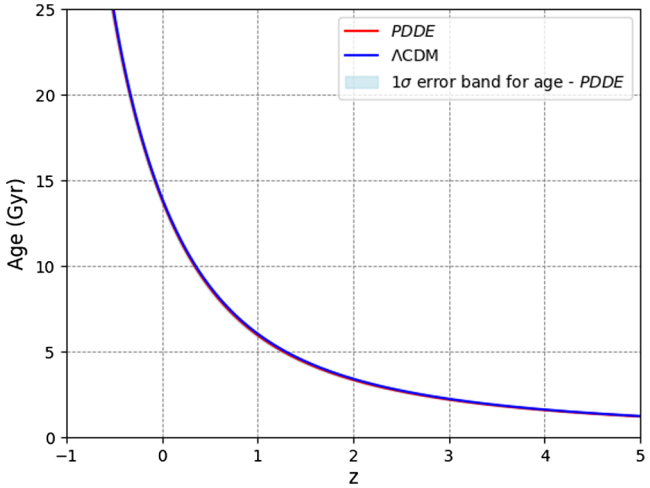

FIG. 3. The age of the universe at each redshift (z) is plotted for the PDDE model with error band and ΛCDM using the best-fit model parameters obtained for the SNIa + BAO + OHD data combination.

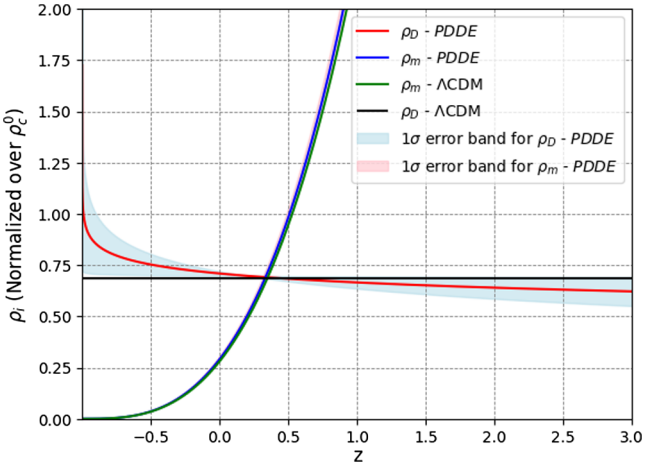

FIG. 4. Evolution of matter density and dark energy density against redshift are plotted for the PDDE model with error band and ΛCDM using the best-fit model parameters obtained for the SNIa + BAO + OHD data combination.

present. However, its evolution shows a considerable difference in the asymptotic future. The ΛCDM model provides a de Sitter solution in the far future evolution while there exists a big-rip singularity where the Hubble parameter blows up for the PDDE model. However, this event is going to happen in the infinite future.

The age of the universe as a function of the scale factor can be obtained as follows. The Hubble parameter, by definition, is $H(a) = \dot{a}/a$, and on rearranging, we get $dt/da = (aH(a))^{-1}$. Hence, the age of the universe at any scale factor a is expressed as

$$t_a - t_B = \int_0^a \frac{1}{aH(a)} da. \tag{14}$$

Here, t_a is the age of the universe at scale factor a, and t_B is the age of the universe at the big bang, which is assumed to be zero. The universe's age with respect to the redshift is plotted in Fig. 3. The present age of the universe is the age at $z = 0$, and the estimated age is 13.86 ± 0.27 Gyr. The age of the universe computed for the ΛCDM model is 13.78 Gyr, and the one that is obtained from the CMB data assuming the standard ΛCDM model [3] is 13.79 Gyr, which are within the 1σ error band of the age predicted by the PDDE model.

Following the individual conservation equation satisfied by matter and dark energy, the evolution of matter energy density is similar to that of the ΛCDM model. The evolution of phantom dynamical dark energy is different from the ΛCDM model. In the ΛCDM model, the dark energy is just the cosmological constant, while phantom dark energy is dynamical. However, the phantom dynamical dark energy density becomes indistinguishable from the cosmological constant at present. The evolution of matter energy density and dark energy density for the PDDE model and ΛCDM model are presented in Fig. 4. The matter density and dark energy density in the ΛCDM model are within the 1σ error band of the PDDE model throughout the late-phase evolution of the universe.

The deceleration parameter (q) characterizes the accelerating or decelerating expansion of the Friedmann-Lemaitre-Robertson-Walker (FLRW) universe. It is expressed as

$$q = -1 - \frac{\dot{H}}{H^2}. \tag{15}$$

It is convenient to express Eq. (15) in terms of dimensionless Hubble parameter $h = H/H_0$ as

$$q = -1 - \frac{1}{2h^2}\frac{dh^2}{dx}, \tag{16}$$

where $\mathbf{x} = \mathbf{ln}(\mathbf{a})$. Substituting for h^2 from Eq. (5), we obtain the deceleration parameter that varies with the scale factor as

$$q = \frac{\Omega_{m_0} a^{-3} - 2\Omega_{D_0} - \Omega_{\text{pdde}}(2\ln a + 1)}{2\Omega_{m_0} a^{-3} + 2\Omega_{D_0} + 2\Omega_{\text{pdde}} \ln a}. \tag{17}$$

The progress of the deceleration parameter with respect to the redshift is plotted in Fig. 5. The positive value of q indicates a decelerating universe, and the universe is accelerating if the value of q is negative. From Fig. 5, it is evident that the universe made a decelerating to accelerating transition. The transition redshift is computed as $z_T = 0.69 \pm 0.03$ while the transition redshift computed for the ΛCDM model using the same dataset combination, SNIa + BAO + OHD is $z_T = 0.70$. It is clear that the value

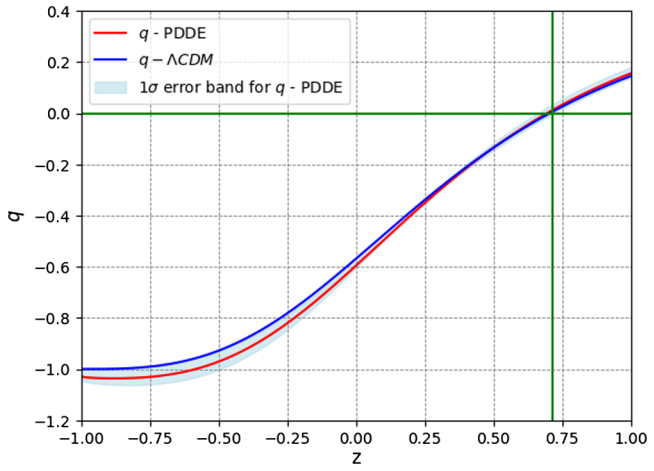

FIG. 5. The progress of deceleration parameter (q) of the universe with respect to redshift (z) is plotted for the PDDE model with error band and ΛCDM using the best-fit model parameters obtained for the SNIa + BAO + OHD data combination. The intersection of the green line represents the present value of the deceleration parameter (q_0).

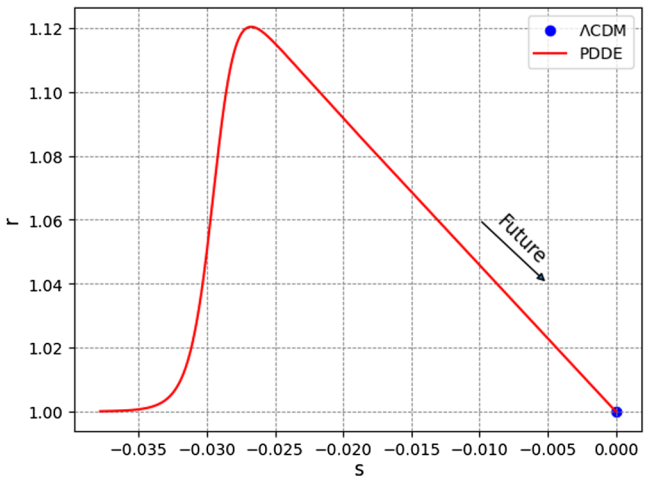

FIG. 6. The statefinder trajectory is plotted for the PDDE model with the model parameters obtained using the SNIa + BAO + OHD data combination. The blue dot represents the ΛCDM fixed point.

obtained for the ΛCDM model is within the 1σ error band of the value obtained using the PDDE model. The present value of the deceleration parameter is $q_0 = -0.59 \pm 0.01$, showing that the universe is accelerating at present. The PDDE model is successful in explaining the recent deceleration to acceleration transition that occurred in the recent past and also the observed present acceleration of the universe.

We compute the statefinder diagnostic pair (r, s), where r is the jerk parameter and s (not the snap parameter) is a parameter constructed out of the jerk parameter and the deceleration parameter to characterize different dark energy models and distinguish between them [85]. The statefinder parameters $r = 1$ and $s = 0$ are a fixed point for the standard ΛCDM model. The jerk parameter is defined as

$$r = \frac{1}{aH^3}\frac{d^3a}{dt^3}. \tag{18}$$

It is convenient to express the r parameter in terms of reduced Hubble parameter $h = H/H_0$; we obtain (for a detailed derivation see Appendix A)

$$r = \frac{1}{2h^2}\frac{d^2h^2}{dx^2} + \frac{3}{2h^2}\frac{dh^2}{dx} + 1, \tag{19}$$

where we have changed the variable from a to $x = \ln a$. The s parameter is defined in terms of the r parameter and the q parameter as

$$s = \frac{r-1}{3(q-\frac{1}{2})}. \tag{20}$$

On expressing s in terms of the reduced Hubble parameter, we get (for a detailed derivation see Appendix A)

$$s = -\frac{\frac{1}{2h^2}\frac{d^2h^2}{dx^2} + \frac{3}{2h^2}\frac{dh^2}{dx}}{\frac{3}{2h^2}\frac{dh^2}{dx} + \frac{9}{2}}. \tag{21}$$

On substituting the expression of h^2 from Eq. (5) in Eqs. (19) and (21), we obtained the evolution of the r and s parameters in the PDDE model as

$$r = \frac{3\Omega_{\text{pdde}}}{2\Omega_{m_0}a^{-3} + 2\Omega_{D_0} + 2\Omega_{\text{pdde}}\ln a} + 1 \tag{22}$$

and

$$s = -\frac{\Omega_{\text{pdde}}}{\Omega_{\text{pdde}} + 3\Omega_{D_0} + 3\Omega_{\text{pdde}}\ln a}. \tag{23}$$

From Eqs. (22) and (23), it is clear that the r and s parameters are dynamical quantities. Also, the parameters $(r, s) = (1, 0)$ are fixed points when $\Omega_{\text{pdde}} = 0$. The r-s trajectory is shown in Fig. 6. It shows that $r > 1$ and $s < 0$ until the trajectory reaches the ΛCDM fixed point that confirms the phantom nature of dark energy density. The present values of r and s are computed as $(r, s) = (1.09, -0.22)$ showing that the PDDE model is distinguishable from the ΛCDM model at present.

V. DYNAMICAL SYSTEM ANALYSIS

Dynamical system analysis is a useful tool in cosmology to extract asymptotic stability of a cosmological model [56,57,86,87]. Fundamental input in dynamical system analysis is the choice of appropriate dynamical variables.

In this study, we consider two dimensionless dynamical variables u and v, defined as

$$u = \frac{\rho_m}{3H^2}, \qquad v = \frac{p_D}{3H^2}. \tag{24}$$

A system of autonomous differential equations can be formulated by taking the derivatives of u and v with respect to the cosmic variable x, and we obtain (for a detailed derivation see Appendix B)

$$\frac{du}{dx} = 3uv = f(u, v), \tag{25}$$

$$\frac{dv}{dx} = 3 - 3u + 6v + 3v^2 = g(u, v). \tag{26}$$

The critical points (u_c, v_c) are obtained by solving the equations $du/dx = 0$ and $dv/dx = 0$, and we get

$$\begin{aligned}(u_c, v_c) &= (1, 0),\\ (u_c, v_c) &= (0, -1).\end{aligned} \tag{27}$$

The stability of the dynamical system near the critical points can be understood by linearizing the system by considering a small variation around the critical points

$$u \to u_c + \delta u, \qquad v \to v_c + \delta v \tag{28}$$

that satisfy the matrix equation

$$\begin{pmatrix}\delta u'\\ \delta v'\end{pmatrix} = \begin{pmatrix}\left(\frac{\partial f}{\partial u}\right)_{u_c,v_c} & \left(\frac{\partial f}{\partial v}\right)_{u_c,v_c}\\ \left(\frac{\partial g}{\partial u}\right)_{u_c,v_c} & \left(\frac{\partial g}{\partial v}\right)_{u_c,v_c}\end{pmatrix}\begin{pmatrix}\delta u\\ \delta v\end{pmatrix}. \tag{29}$$

The Jacobian matrix given in Eq. (29) evaluated at the critical points (1, 0) and $(0, -1)$, respectively, are

$$J_{(1,0)} = \begin{pmatrix}0 & 3\\ -3 & 6\end{pmatrix}, \qquad J_{(0,-1)} = \begin{pmatrix}-3 & 0\\ -3 & 0\end{pmatrix}. \tag{30}$$

The stability of the critical points is determined by the eigenvalues of the matrix J. If both of the eigenvalues are negative, the critical point is a future attractor that is asymptotically stable. All the trajectories near the critical point approach that point. If both the eigenvalues are positive, the critical point is a past-time attractor or an unstable equilibrium point. All the trajectories near the critical point will be repelled from the point. If one eigenvalue is positive and the other negative, the critical point is a saddle point. Some trajectories will be attracted to the critical point while others will repel. If one of the eigenvalue is positive and the other zero, the critical point is unstable. The positive eigenvalue guarantees that there exist at least one unstable direction. If one of the eigenvalue is zero and the other is negative, the linear stability theory cannot explain the stability of the critical point. If both eigenvalues are complex numbers of the form $\beta + i\gamma$ and $\beta - i\gamma$ with $\beta > 0$ and $\gamma \neq 0$, the critical point is an unstable spiral. If $\beta < 0$ and $\gamma \neq 0$, the critical point is a stable spiral. If $\beta = 0$, the critical point is called a center and the solutions are oscillatory [58]. Diagonalizing $J_{(1,0)}$ and $J_{(0,-1)}$, we obtained the eigenvalues that correspond to the critical points (1, 0) and $(0, -1)$ as (3, 3) and $(-3, 0)$, respectively. The critical point $(\rho_m/3H^2, p_D/3H^2) = (1, 0)$ corresponds to a fixed point in the matter dominated phase. Since both the eigenvalues are positive, it represents an unstable equilibrium point. The critical point $(\rho_m/3H^2, p_D/3H^2) = (0, -1)$ corresponds to a fixed point in the far future where matter density is zero and the universe is completely occupied with vacuum energy. The stability of this critical point cannot be determined by analyzing the eigenvalue as the point is nonhyperbolic. The phase space portrait of the dynamical system is shown in Fig. 7. From Fig. 7, it is evident that the critical point (1, 0) is an unstable equilibrium point so that all the trajectories in the neighborhood of this point are repelled out from the point. However, the stability of the critical point $(0, -1)$ cannot be inferred from the phase space plot. Here, the linear stability analysis fails to explain the stability of the critical point. Hence, we use the center manifold theory to simplify the system by reducing the dimensionality [58,61,88].

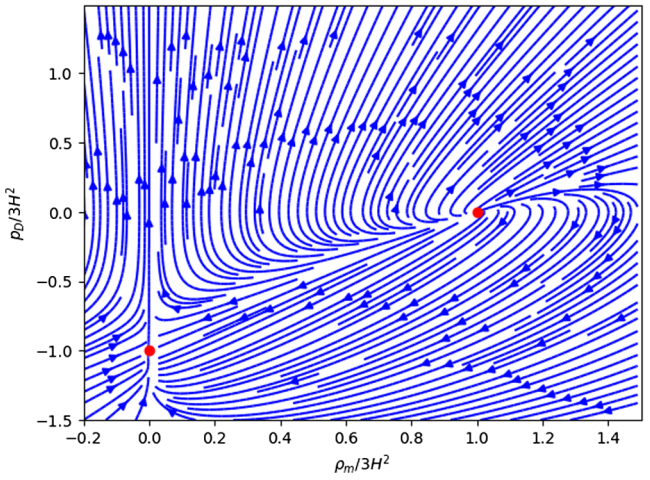

FIG. 7. The phase space trajectory in the $(\rho_m/3H^2)$-$(p_D/3H^2)$ plane for the PDDE model. The red dots represent the critical points.

The model has a critical point at $(0, -1)$ with eigenvalues $(-3, 0)$. To use the central manifold theory, we shift the point to the origin or equivalently transform Eqs. (25) and (B13) into a set of new variables given by

$$U = u, \qquad V = v + 1. \tag{31}$$

Then, Eqs. (25) and (B13) can be rewritten as

$$\frac{dU}{dx} = 3UV - 3U, \tag{32}$$

$$\frac{dV}{dx} = 3V^2 - 3U. \tag{33}$$

The Jacobian matrix for the system can be expressed as

$$J = \begin{pmatrix} 3V-3 & 3U \\ -3 & 6V \end{pmatrix}. \tag{34}$$

The Jacobian matrix for the critical point (0, 0) is

$$J|_{U=0,V=0} = \begin{pmatrix} -3 & 0 \\ -3 & 0 \end{pmatrix}. \tag{35}$$

Now, we construct another set of variables (X, Y) defined as

$$\begin{pmatrix} X \\ Y \end{pmatrix} = S^{-1} \begin{pmatrix} U \\ V \end{pmatrix}, \tag{36}$$

where S is the inverse of the diagonalizing matrix constructed out of the eigenvectors of the matrix $J|_{U=0,V=0}$. The matrix S obtained is

$$S = \begin{pmatrix} 0 & 1 \\ 1 & 1 \end{pmatrix}. \tag{37}$$

Now, it is possible to express U and V in terms of new dynamical variables X and Y as

$$V = X + Y, \qquad U = Y. \tag{38}$$

Then, Eqs. (32) and (33) can be expressed in terms of the new variables X and Y as

$$\dot{X} = 3X^2 + 3XY, \tag{39}$$

$$\dot{Y} = 3XY + 3Y^2 - 3Y, \tag{40}$$

which according to central manifold theory can be represented as

$$\dot{X} = AX + F(X, Y), \tag{41}$$

$$\dot{Y} = BY + G(X, Y). \tag{42}$$

Comparing Eqs. (39) and (41), we obtain $A = 0$ and $F(X, Y) = 3X^2 + 3XY$. Similarly, from Eqs. (40) and (42) we obtain $B = -3$ and $G(X, Y) = 3XY + 3Y^2$. Assuming $\mathbf{Y} = \mathbf{p}(\mathbf{X})$, for $p(X)$ to be the center manifold, it satisfies the quasilinear partial differential equation

$$\frac{dp(X)}{dX}[AX + F(X, p(X))] - Bp(X) - G(X, p(X)) = 0. \tag{43}$$

The above equation is difficult to solve using the standard method. Therefore, we Taylor expand the center manifold $p(X)$ around $X = 0$ [89]. The major limitations to this power series expansion is that the series often diverge. However, an exact knowledge of the center manifold p is not required for this equilibrium analysis, since it is frequently sufficient to compute only the low degree terms of the Taylor series expansion of p around $X = 0$ [90]. This allows us to determine the stability of the system. To proceed with determining the center manifold, it is customary to suppose the expansion for $p(X)$ of the form

$$p(X) = a_2X^2 + a_3X^3 + \mathcal{O}(X^4). \tag{44}$$

Substituting Eq. (44) into Eq. (43), we obtain

$$(2a_2X + 3a_3X^2)(3X^2 + 3X(a_2X^2 + a_3X^3)) - 3X(a_2X^2 + a_3X^3) - 3(a_2X^2 + a_3X^3)^2 + 3(a_2X^2 + a_3X^3) = 0. \tag{45}$$

For Eq. (45) to hold, the coefficient of each powers of X must be zero. Then, we get the coefficients $a_2 = 0$, $a_3 = 0$, and hence $p(X) = \mathcal{O}(X^4)$. Then, the dynamical system restricted to the center manifold is expressed as

$$\dot{X} = 3X^2 + \mathbf{O}(X^5). \tag{46}$$

From Eq. (46), it can be concluded that for sufficiently small X, $X \to 0$, the system is unstable. Hence, the critical point (0, 0) is unstable. The analysis shows that there is no stable equilibrium point existing in any evolutionary stage of the universe. Hence, we conclude that the universe is dynamically unstable within the PDDE model. It should be noted that the universe is dynamically stable and will attain a de Sitter evolution in the far future within the ΛCDM model. Hence, we conclude that, even though the present model alleviates the Hubble tension to some extent, the model is not dynamically stable and hence may not be considered as a potential alternate to the ΛCDM model.

VI. EVOLUTION OF HORIZON ENTROPY AND GSL

It was Bekenstein and Hawking who showed that the entropy of black holes is directly proportional to the area of

their event horizon [70,71,91]. The event horizon entropy ($S_{\rm EH}$) is given by

$$S_{\rm EH} = \frac{A_{\rm EH}}{4l_p^2} k_B, \tag{47}$$

where $A_{\rm EH}$ is the area of the event horizon, l_p is the Planck length, and k_B is the Boltzmann constant. Later, Gibbons and Hawking showed that the cosmological horizon also possesses entropy proportional to the area [72,92]. Instead of the event horizon, the Hubble horizon is mostly used to estimate horizon entropy because it provides the observable boundary at present. Hence, the area-entropy relation for the observable universe can be expressed as

$$S_H = \frac{A_H}{4l_p^2} k_B, \tag{48}$$

where $A_H = 4\pi c^2/H^2$ is the area of the Hubble horizon. According to the generalized second law of thermodynamics (GSL), the entropy of the universe (horizon entropy + entropy of its interior) must be a never decreasing function of time [71,93],

$$\dot{S} = \dot{S}_H + \dot{S}_m \geq 0, \tag{49}$$

where S_m is the entropy contribution from anything present inside the Hubble horizon and the overdot denotes the derivative with respect to the cosmic time. In general, the S_m include entropy contributions from baryon matter ($S_b \sim 10^{81} k_B$), dark matter ($S_{dm} \sim 10^{88\pm1} k_B$), photons ($S_{\rm rad} \sim 10^{89} k_B$), relic neutrinos ($S_\nu \sim 10^{89} k_B$), relic gravitons ($S_{\rm grav} \sim 10^{87} k_B$), stellar black holes ($S_{SBH} \sim 10^{97} k_B$), and supermassive black holes ($S_{SMBH} \sim 10^{104} k_B$). However, the horizon entropy ($S_H \sim 10^{122} k_B$) is very much higher than that of the entropy contribution due to any of the cosmic components mentioned above [94]. Hence, we consider only the horizon entropy for the following discussions. The horizon entropy is obtained by substituting the expression of the horizon area into Eq. (48), and we obtain

$$S_H = \frac{\pi c^2}{l_p^2 H^2} k_B, \tag{50}$$

where the evolution of the Hubble parameter is given by Eq. (5). The derivative of the horizon entropy with respect to the scale factor is obtained as

$$S'_H = \frac{\pi c^2 k_B}{l_p^2 H_0^2} \left(\frac{3\Omega_{m_0} a^{-4} - \Omega_{\rm pdde} a^{-1}}{h^4} \right). \tag{51}$$

To check the convexity condition of entropy, we also obtained the expression for the second derivative of entropy with respect to the scale factor,

$$S''_H = \frac{\pi c^2 k_B}{l_p^2 H_0^2} \left[-\frac{1}{h^4} (12\Omega_{m_0} a^{-5} - \Omega_{\rm pdde} a^{-2}) + \frac{2}{h^6} (3\Omega_{m_0} a^{-4} - \Omega_{\rm pdde} a^{-1})^2 \right]. \tag{52}$$

The evolution of S_H (blue curve), S'_H (green curve), and S''_H (red curve) are depicted in Fig. 8. From Fig. 8, it is conclusive that entropy decreases with respect to the scale factor in the far future evolution. However, it is not evident from the S'_H and S''_H curves. To show this behavior more explicitly, we zoomed the individual curve in the region between $z = -1$ and $z = -0.5$, and the plots are shown in Figs. 9 and 10. From Fig. 9, it is clear that dS_H/da has positive and negative values. But, according to GSL, $dS_H/da \geq 0$ throughout the evolution. A negative value of dS_H/da in the later stage of evolution is a clear violation of GSL. Furthermore, it is well-known that any isolated system evolves toward a state of maximum entropy. In other words, the entropy should be a convex function of the scale factor, that is,

$$S''_H < 0, \tag{53}$$

at least in the later stage of evolution. Figure 10 shows that the convexity condition for a redshift range in the late accelerating phase is not satisfied. In this region, the second S''_H attains a maximum positive value and then approaches zero from above. The entropy is not bounded from below.

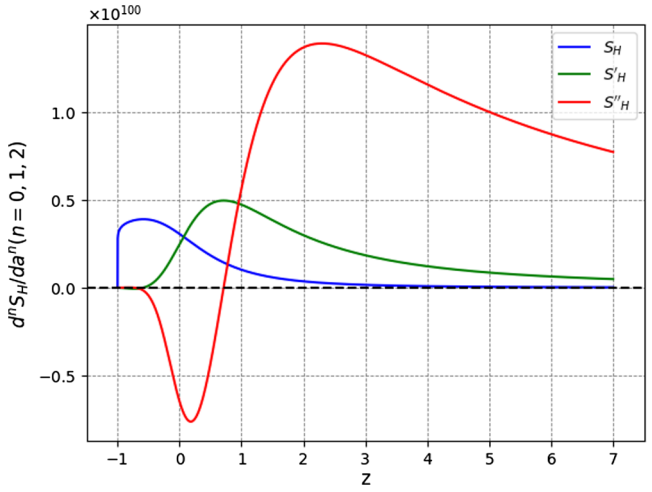

FIG. 8. Evolution of horizon entropy (S_H) and first and second derivatives (S'_H and S''_H) of horizon entropy against redshift.

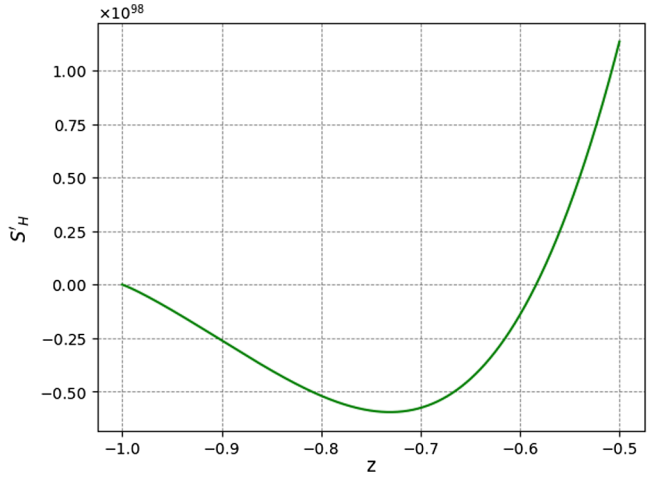

FIG. 9. The change in horizon entropy (S'_H) is plotted against the redshift and zoomed to explicitly show the violation of the generalized second law of thermodynamics.

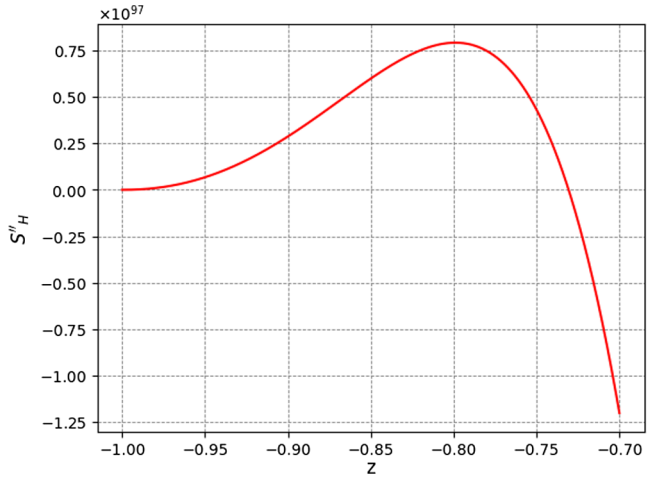

FIG. 10. The second derivative of entropy with respect to the scale factor (S''_H) is plotted against the redshift and zoomed to explicitly show that the PDDE model does not satisfy the convexity condition.

This implies that the entropy evolution of the universe within the PDDE model does not behave as an ordinary macroscopic system. In conclusion, the PDDE model violates the generalized second law of thermodynamics and is inconsistent with entropy maximization.

VII. CONCLUSION

In the present work, we examine the dynamical stability of the PDDE model and its thermodynamic consistency. The PDDE model, also termed the little sibling of the big rip, is a new event smoother than the existing big rip singularities within the phantom dark energy models. This event happens at $a \to \infty$ when the scalar curvature explodes. When this event is reached, the scale factor and the Hubble parameter diverge while the derivative of the Hubble parameter remains finite. The model behaves like ΛCDM at present. However, the universe would not be asymptotic de Sitter as in the ΛCDM model [41]. We performed parameter inference of the model based on MCMC using a string of observations SNIa + BAO + OHD. Our analysis shows that the model agrees with the observational data. The best-fit values of the model parameters obtained are $H_0 = 68.86 \pm 0.5746\ \mathrm{km\,s^{-1}\,Mpc^{-1}}$, $\Omega_{m_0} = 0.291 \pm 0.011$, and $\Omega_{\mathrm{pdde}} = 0.063 \pm 0.059$. These values are consistent with those reported by Bouali *et al.* [42]. It should be noted that the standard deviation obtained for the parameter Ω_{pdde} is almost equal to the best-fit value. This implies that the data prefer the nonzero value of Ω_{pdde} at a significance of $\sim 1\sigma$, which is statistically less significant.

The universe's age is computed as 13.86 ± 0.27 Gyr, consistent with the standard model prediction. The evolution of matter density in the PDDE model is the same as that in the ΛCDM model. In contrast, the dark energy density is not just a cosmological constant but instead varies with time. The present value of the deceleration parameter is negative, showing that the universe is accelerating at present. The decelerating universe recently transitioned into the accelerating phase at a redshift $z_T = 0.69 \pm 0.03$. The statefinder parameter distinguished the PDDE model from the ΛCDM model, and the $r - s$ trajectory reveals the phantom nature of dark energy density.

We performed the dynamical system analysis to test the dynamical stability of the PDDE model. We obtained two critical points on solving autonomous coupled differential equations that are satisfied by the dynamical variables, $\rho_m/3H^2$ and $p_D/3H^2$, and we obtained two critical points $(1, 0)$ and $(0, -1)$. The point $(1, 0)$ is a fixed point in the matter dominated phase and $(0, -1)$ is a fixed point in the late accelerating phase. The eigenvalues obtained by diagonalizing the Jacobian matrices are $(3, 3)$ and $(-3, 0)$ for the critical points $(1, 0)$ and $(0, -1)$, respectively. The fixed point $(1, 0)$ is an unstable equilibrium point and $(0, -1)$ is a saddle point that is also unstable. In conclusion, the universe is dynamically unstable in the matter dominated epoch and late accelerating epoch within the PDDE model.

We assessed the validity of GSL in the PDDE model by prioritizing the horizon entropy over other cosmic components [94]. Our study, by considering the Hubble horizon as the thermodynamic boundary shows that the horizon entropy is a nonincreasing function of cosmic time for the PDDE dominated universe. Further, our result shows that the entropy is not bounded from below for a range of redshift in the future evolution; hence, the model does not satisfy the entropy maximization. The universe does not behave as an ordinary macroscopic system within the PDDE model. However, the conditions for validity of GSL in a universe dominated with phantom energy is

discussed in Refs. [73,95,96]. In phantom cosmologies, the violation of dominant energy condition $(p+\rho)<0$ and assuming Euler's relation $Ts=p+\rho$ leads to either negative entropy of the universe or negative temperature. However, the use of negative temperature and positive entropy leads to violation of GSL within the phantom universe, which is discussed in Ref. [95]. Assuming the accelerated universe that is filled with a perfect fluid satisfying the first law of thermodynamics and considering the temperature proportional to the de Sitter temperature, they have shown that the positivity of the temperature is the necessary condition to satisfy GSL.

In summary, the model is dynamically unstable and thermodynamically inconsistent despite the present model being in good agreement with the observational data and a potential candidate to smoothen the Hubble tension. Our analysis shows that the PDDE model may not be considered a possible alternative to the standard model of cosmology, the ΛCDM.

In this study, we assumed no interaction between dark matter and dark energy. However, by introducing a potential energy exchange term between these dark sectors, we can assess the model's dynamical stability. It has been shown in Refs. [53,54,97] that the phantom dark energy model with interaction between dark sectors exhibits dynamical stability. Furthermore, the phantom field model presented in [55] also exhibits dynamical stability in the presence of bulk viscous dark matter where dark matter and dark energy are interacting, provided the temperature of the fluid is less than or equal to the de Sitter temperature. Hence, the present study can be extended by incorporating the interaction term and bulk viscosity in the matter sector, and one can check the possibility of a stable fixed point in the far future evolution of the universe and also the validity of GSL.

ACKNOWLEDGMENTS

One of the authors (S. N.) acknowledges Indian Institute of Technology Kanpur for providing the Institute postdoctoral fellowship. The authors acknowledge the central computational facility, Center of Excellence in Environment, Government Brennen College, Thalassery, for providing the high-end system to perform computational tasks. The authors thank Sanitha A, Manosh T.M, and Amalendu Raghunath for suggestions on the manuscript.

APPENDIX A: DETAILED CALCULATION OF q, r, AND s PARAMETERS IN TERMS OF REDUCED HUBBLE PARAMETER (h)

The Hubble parameter (H), the deceleration parameter (q), and the jerk parameter (r) are defined as

$$H(t)=\frac{1}{a}\frac{da}{dt}, \tag{A1}$$

$$q(t)=-\frac{1}{a}\frac{d^2a}{dt^2}\left[\frac{1}{a}\frac{da}{dt}\right]^{-2}, \tag{A2}$$

$$r(t)=\frac{1}{a}\frac{d^3a}{dt^3}\left[\frac{1}{a}\frac{da}{dt}\right]^{-3}. \tag{A3}$$

Equation (A2) is rewritten as

$$q(t)=-\frac{1}{a}\frac{d\dot{a}}{dt}[H]^{-2}, \tag{A4}$$

and substituting for $\dot{a}=aH$, we obtain

$$q(t)=-\frac{1}{a}\frac{d(aH)}{dt}[H]^{-2}. \tag{A5}$$

Using the product rule of differentiation, we obtain

$$q(t)=-\frac{1}{a}(H\dot{a}+a\dot{H})[H]^{-2}, \tag{A6}$$

which can be further reduced to

$$q=-\left[1+\frac{1}{H^2}\frac{dH}{dt}\right]. \tag{A7}$$

On changing the variable from t to x, where $x=\ln a$, we obtain

$$q=-1-\frac{1}{2H^2}\frac{dH^2}{dx}. \tag{A8}$$

The Hubble parameter H can be expressed in terms of reduced Hubble parameter h as $H=H_0h$, and then we obtain

$$q=-1-\frac{1}{2h^2}\frac{dh^2}{dx}. \tag{A9}$$

Similar calculation is done to obtain the r parameter in terms of h as follows. Equation (A3) can be written as

$$r(t)=\frac{1}{a}\frac{d^2\dot{a}}{dt^2}[H]^{-3}. \tag{A10}$$

Substituting for $\dot{a}=aH$ and using the product rule of differentiation, we obtain

$$r=1+\frac{3}{H^2}\frac{dH}{dt}+\frac{1}{H^3}\frac{d}{dt}\frac{dH}{dt}. \tag{A11}$$

On changing the variable from t to x, we obtain

$$r=1+\frac{3}{2H^2}\frac{dH^2}{dx}+\frac{1}{2H^2}\frac{d^2H^2}{dx^2}. \tag{A12}$$

We can further express Eq. (A12) in terms of h as

$$r = 1 + \frac{3}{2h^2}\frac{dh^2}{dx} + \frac{1}{2h^2}\frac{d^2h^2}{dx^2}. \tag{A13}$$

By definition, the s parameter is [85]

$$s = \frac{r-1}{3(q-\frac{1}{2})}. \tag{A14}$$

Substituting the expression of r from Eq. (A12) and q from Eq. (A9), we obtain

$$s = -\frac{\frac{3}{2h^2}\frac{dh^2}{dx} + \frac{1}{2h^2}\frac{d^2h^2}{dx^2}}{\frac{3}{2h^2}\frac{dh^2}{dx} + \frac{9}{2}}. \tag{A15}$$

APPENDIX B: DETAILED DERIVATION OF AUTONOMOUS DIFFERENTIAL EQUATIONS FOR THE DYNAMICAL SYSTEM ANALYSIS

We define two dimensionless dynamical variables u and v as

$$u = \frac{\rho_m}{3H^2}, \qquad v = \frac{p_D}{3H^2}. \tag{B1}$$

On taking the derivative of u with respect to x, where $x = \ln a$, we obtain

$$\frac{du}{dx} = \frac{3H^2\frac{d\rho_m}{dx} - \rho_m\frac{3H^2}{dx}}{(3H^2)^2}. \tag{B2}$$

Using the Friedmann equation,

$$3H^2 = \rho_m + \rho_D, \tag{B3}$$

where we assumed $8\pi G = 1$, we can express Eq. (B2) as

$$\frac{du}{dx} = \frac{3H^2\frac{d\rho_m}{dx} - \rho_m\frac{d(\rho_m+\rho_D)}{dx}}{(3H^2)^2}. \tag{B4}$$

The conservation equation for pressureless matter (ω_m) is

$$\dot{\rho}_m + 3H\rho_m = 0. \tag{B5}$$

On changing the variable from t to x, where $x = \ln a$, we obtain

$$\frac{d\rho_m}{dx} = -3\rho_m. \tag{B6}$$

In the PDDE model, the dark energy density has the form

$$\rho_D(a) = \rho_{D,0} + \alpha \ln a. \tag{B7}$$

The conservation equation satisfied by the PDDE is

$$\dot{\rho_D} + 3H(\rho_D + p_D) = 0. \tag{B8}$$

Hence, the dark energy density and the corresponding pressure are related through the expression

$$\rho_D + p_D = -\frac{\alpha}{3}. \tag{B9}$$

From Eq. (B7), it is evident that

$$\frac{d\rho_D}{dx} = \frac{d(\rho_{D,0} + \alpha \ln a)}{dx} = \alpha. \tag{B10}$$

Substituting Eqs. (B6) and (B10) in Eq. (B4), we get

$$\frac{du}{dx} = \frac{3H^2(-3\rho_m) - \rho_m(-3\rho_m + \alpha)}{(3H^2)^2}. \tag{B11}$$

Using Eqs. (B3) and (B9), we can express the parameter α in terms of matter density and dark energy density as

$$\alpha = -3p_D - 9H^2 + 3\rho_m. \tag{B12}$$

Substituting the value of α in Eq. (B11) and simplifying we get

$$\frac{du}{dx} = 3uv. \tag{B13}$$

Similarly,

$$\frac{dv}{dx} = \frac{d}{dx}\left(\frac{p_D}{3H^2}\right), \tag{B14}$$

i.e.,

$$\frac{dv}{dx} = \frac{3H^2\frac{dp_D}{dx} - p_D\frac{d(\rho_m+\rho_D)}{dx}}{(3H^2)^2}. \tag{B15}$$

However,

$$\frac{dp_D}{dx} = -\frac{d\rho_D}{dx} = -\alpha. \tag{B16}$$

Substituting Eqs. (B6), (B10), and (B16) in Eq. (B15), we get

$$\frac{dv}{dx} = 3 - 3u + 6v + 3v^2. \tag{B17}$$

[1] S. Perlmutter, G. Aldering, G. Goldhaber, R. Knop, P. Nugent, P. G. Castro, S. Deustua, S. Fabbro, A. Goobar, D. E. Groom *et al.*, Astrophys. J. **517**, 565 (1999).

[2] A. G. Riess, A. V. Filippenko, P. Challis, A. Clocchiatti, A. Diercks, P. M. Garnavich, R. L. Gilliland, C. J. Hogan, S. Jha, R. P. Kirshner *et al.*, Astrophys. J. **116**, 1009 (1998).

[3] N. Aghanim, Y. Akrami, M. Ashdown, J. Aumont, C. Baccigalupi, M. Ballardini, A. Banday, R. Barreiro, N. Bartolo, S. Basak *et al.*, Astron. Astrophys. **641**, A6 (2020).

[4] M. Tegmark, M. A. Strauss, M. R. Blanton, K. Abazajian, S. Dodelson, H. Sandvik, X. Wang, D. H. Weinberg, I. Zehavi, N. A. Bahcall *et al.*, Phys. Rev. D **69**, 103501 (2004).

[5] D. N. Spergel, L. Verde, H. V. Peiris, E. Komatsu, M. Nolta, C. L. Bennett, M. Halpern, G. Hinshaw, N. Jarosik, A. Kogut *et al.*, Astrophys. J. Suppl. Ser. **148**, 175 (2003).

[6] G. F. Smoot, C. L. Bennett, A. Kogut, E. Wright, J. Aymon, N. Boggess, E. Cheng, G. De Amici, S. Gulkis, M. Hauser *et al.*, Astrophys. J. **396**, L1 (1992).

[7] P. A. Ade, N. Aghanim, C. Armitage-Caplan, M. Arnaud, M. Ashdown, F. Atrio-Barandela, J. Aumont, C. Baccigalupi, A. J. Banday, R. Barreiro *et al.*, Astron. Astrophys. **571**, A16 (2014).

[8] D. J. Eisenstein, I. Zehavi, D. W. Hogg, R. Scoccimarro, M. R. Blanton, R. C. Nichol, R. Scranton, H.-J. Seo, M. Tegmark, Z. Zheng *et al.*, Astrophys. J. **633**, 560 (2005).

[9] P. A. Ade, N. Aghanim, M. Arnaud, M. Ashdown, J. Aumont, C. Baccigalupi, A. Banday, R. Barreiro, J. Bartlett, N. Bartolo *et al.*, Astron. Astrophys. **594**, A13 (2016).

[10] P. J. E. Peebles and B. Ratra, Rev. Mod. Phys. **75**, 559 (2003).

[11] P. J. E. Peebles, *Principles of Physical Cosmology* (Princeton University Press, Princeton, NJ, 1993), Vol. 27.

[12] S. Weinberg, Rev. Mod. Phys. **61**, 1 (1989).

[13] H. E. Velten, R. Vom Marttens, and W. Zimdahl, Eur. Phys. J. C **74**, 1 (2014).

[14] A. G. Riess, S. Casertano, W. Yuan, J. B. Bowers, L. Macri, J. C. Zinn, and D. Scolnic, Astrophys. J. Lett. **908**, L6 (2021).

[15] A. G. Riess, S. Casertano, W. Yuan, L. M. Macri, and D. Scolnic, Astrophys. J. **876**, 85 (2019).

[16] S. Joudaki, H. Hildebrandt, D. Traykova, N. Chisari, C. Heymans, A. Kannawadi, K. Kuijken, A. Wright, M. Asgari, T. Erben *et al.*, Astron. Astrophys. **638**, L1 (2020).

[17] S. D. Odintsov, D. S.-C. Gómez, and G. S. Sharov, Nucl. Phys. **B966**, 115377 (2021).

[18] T. Schiavone, G. Montani, and F. Bombacigno, Mon. Not. R. Astron. Soc. **522**, L72 (2023).

[19] S. A. Adil, M. R. Gangopadhyay, M. Sami, and M. K. Sharma, Phys. Rev. D **104**, 103534 (2021).

[20] S. Nojiri, S. Odintsov, and V. Oikonomou, Nucl. Phys. **B980**, 115850 (2022).

[21] E. Di Valentino, O. Mena, S. Pan, L. Visinelli, W. Yang, A. Melchiorri, D. F. Mota, A. G. Riess, and J. Silk, Classical Quantum Gravity **38**, 153001 (2021).

[22] S. Pan, W. Yang, E. Di Valentino, E. N. Saridakis, and S. Chakraborty, Phys. Rev. D **100**, 103520 (2019).

[23] T. Karwal, M. Raveri, B. Jain, J. Khoury, and M. Trodden, Phys. Rev. D **105**, 063535 (2022).

[24] R. Murgia, G. F. Abellán, and V. Poulin, Phys. Rev. D **103**, 063502 (2021).

[25] F. Niedermann and M. S. Sloth, Phys. Rev. D **102**, 063527 (2020).

[26] K. Bamba, S. Capozziello, S. Nojiri, and S. D. Odintsov, Astrophys. Space Sci. **342**, 155 (2012).

[27] E. Ó. Colgáin and M. Sheikh-Jabbari, Classical Quantum Gravity **38**, 177001 (2021).

[28] J. S. Peracaula, A. Gómez-Valent, J. de Cruz Pérez, and C. Moreno-Pulido, Europhys. Lett. **134**, 19001 (2021).

[29] C. Krishnan, E. Ó. Colgáin, M. Sheikh-Jabbari, and T. Yang, Phys. Rev. D **103**, 103509 (2021).

[30] W.-M. Dai, Y.-Z. Ma, and H.-J. He, Phys. Rev. D **102**, 121302 (2020).

[31] M. H. Van Putten, Astrophys. J. **848**, 28 (2017).

[32] V. Poulin, T. L. Smith, T. Karwal, and M. Kamionkowski, Phys. Rev. Lett. **122**, 221301 (2019).

[33] S. Nojiri, S. D. Odintsov, D. S.-C. Gómez, and G. S. Sharov, Phys. Dark Universe **32**, 100837 (2021).

[34] G. Acquaviva, Ö. Akarsu, N. Katırcı, and J. A. Vazquez, Phys. Rev. D **104**, 023505 (2021).

[35] M. Malekjani, R. M. Conville, E. Ó. Colgáin, S. Pourojaghi, and M. Sheikh-Jabbari, arXiv:2301.12725.

[36] X. Li and A. Shafieloo, Astrophys. J. Lett. **883**, L3 (2019).

[37] M. Rezaei, T. Naderi, M. Malekjani, and A. Mehrabi, Eur. Phys. J. C. **80**, 374 (2020).

[38] E. Ó. Colgáin, M. Sheikh-Jabbari, R. Solomon, M. G. Dainotti, and D. Stojkovic, arXiv:2206.11447.

[39] S. A. Adil, Ö. Akarsu, M. Malekjani, E. Ó. Colgáin, S. Pourojaghi, A. A. Sen, and M. Sheikh-Jabbari, arXiv:2303.06928.

[40] M. Esposito, V. Iršič, M. Costanzi, S. Borgani, A. Saro, and M. Viel, Mon. Not. R. Astron. Soc. **515**, 857 (2022).

[41] M. Bouhmadi-Lopez, A. Errahmani, P. Martin-Moruno, T. Ouali, and Y. Tavakoli, Int. J. Mod. Phys. D **24**, 1550078 (2015).

[42] A. Bouali, I. Albarran, M. Bouhmadi-López, and T. Ouali, Phys. Dark Universe **26**, 100391 (2019).

[43] A. Bouali, I. Albarran, M. Bouhmadi-López, A. Errahmani, and T. Ouali, Phys. Dark Universe **34**, 100907 (2021).

[44] S. Dahmani, A. Bouali, I. E. Bojaddaini, A. Errahmani, and T. Ouali, arXiv:2301.04200.

[45] D. M. Scolnic, D. Jones, A. Rest, Y. Pan, R. Chornock, R. Foley, M. Huber, R. Kessler, G. Narayan, A. Riess *et al.*, Astrophys. J. **859**, 101 (2018).

[46] S. M. Carroll, M. Hoffman, and M. Trodden, Phys. Rev. D **68**, 023509 (2003).

[47] V. B. Johri, Phys. Rev. D **70**, 041303 (2004).

[48] A. Vikman, Phys. Rev. D **71**, 023515 (2005).

[49] R. John, N. Sarath, and T. K. Mathew, Eur. Phys. J. C **83**, 697 (2023).

[50] S. W. Hawking and G. F. Ellis, *The Large Scale Structure of Space-Time* (Cambridge University Press, Cambridge, England, 2023).

[51] R. M. Wald, *General Relativity* (University of Chicago Press, Chicago, 2010).

[52] N. Cruz, S. Lepe, Y. Leyva, F. Pena, and J. Saavedra, Phys. Rev. D **90**, 083524 (2014).

[53] R. Curbelo, T. Gonzalez, G. León, and I. Quiros, Classical Quantum Gravity **23**, 1585 (2006).

[54] X.-m. Chen, Y. Gong, and E. N. Saridakis, J. Cosmol. Astropart. Phys. 04 (2009) 001.

[55] M. Sharif and Q. Ama-Tul-Mughani, Universe **5**, 185 (2019).
[56] J. Wainwright and G. F. R. Ellis, *Dynamical Systems in Cosmology* (Cambridge University Press, Cambridge, England, 1997).
[57] A. A. Coley, *Dynamical Systems and Cosmology* (Springer Science & Business Media, Berlin, Germany, 2003), Vol. 291.
[58] C. G. Böhmer and N. Chan, in *Dynamical and Complex Systems* (World Scientific, Singapore, 2017), pp. 121–156.
[59] C. G. Boehmer, N. Chan, and R. Lazkoz, Phys. Lett. B **714**, 11 (2012).
[60] R. Raushan, S. Angit, and R. Chaubey, Eur. Phys. J. Plus **136**, 440 (2021).
[61] S. Bahamonde, C. G. Böhmer, S. Carloni, E. J. Copeland, W. Fang, and N. Tamanini, Phys. Rep. **775–777**, 1 (2018).
[62] P. C. Davies, Classical Quantum Gravity **4**, L225 (1987).
[63] R. Brustein, Phys. Rev. Lett. **84**, 2072 (2000).
[64] M. Li, Phys. Lett. B **603**, 1 (2004).
[65] P. F. Gonzalez-Diaz, arXiv:hep-th/0411070.
[66] R. Bousso, Phys. Rev. D **71**, 064024 (2005).
[67] H. M. Sadjadi, Phys. Lett. B **645**, 108 (2007).
[68] V. F. Cardone, N. Radicella, and A. Troisi, Entropy **19**, 392 (2017).
[69] S. W. Hawking, Commun. Math. Phys. **43**, 199 (1975).
[70] J. D. Bekenstein, Phys. Rev. D **7**, 2333 (1973).
[71] J. D. Bekenstein, Phys. Rev. D **9**, 3292 (1974).
[72] G. W. Gibbons and S. W. Hawking, Phys. Rev. D **15**, 2738 (1977).
[73] M. Jamil, E. N. Saridakis, and M. Setare, Phys. Rev. D **81**, 023007 (2010).
[74] R. Trotta, Contemp. Phys. **49**, 71 (2008).
[75] S. Alam, M. Ata, S. Bailey, F. Beutler, D. Bizyaev, J. A. Blazek, A. S. Bolton, J. R. Brownstein, A. Burden, C.-H. Chuang *et al.*, Mon. Not. R. Astron. Soc. **470**, 2617 (2017).
[76] V. de Sainte Agathe, C. Balland, H. D. M. Des Bourboux, M. Blomqvist, J. Guy, J. Rich, A. Font-Ribera, M. M. Pieri, J. E. Bautista, K. Dawson *et al.*, Astron. Astrophys. **629**, A85 (2019).
[77] S. Cao, J. Ryan, and B. Ratra, Mon. Not. R. Astron. Soc. **497**, 3191 (2020).
[78] J. Ryan, Y. Chen, and B. Ratra, Mon. Not. R. Astron. Soc. **488**, 3844 (2019).
[79] X. Zheng, X. Ding, M. Biesiada, S. Cao, and Z. Zhu, Astrophys. J. **825**, 17 (2016).
[80] Y. Lian, S. Cao, M. Biesiada, Y. Chen, Y. Zhang, and W. Guo, Mon. Not. R. Astron. Soc. **505**, 2111 (2021).
[81] T. Faerber and M. López-Corredoira, Universe **6**, 114 (2020).
[82] R. Andrae, T. Schulze-Hartung, and P. Melchior, arXiv: 1012.3754.
[83] O. Farooq, F. R. Madiyar, S. Crandall, and B. Ratra, Astrophys. J. **835**, 26 (2017).
[84] D. Foreman-Mackey, D. W. Hogg, D. Lang, and J. Goodman, Publ. Astron. Soc. Pac. **125**, 306 (2013).
[85] V. Sahni, T. D. Saini, A. A. Starobinsky, and U. Alam, JETP Lett. **77**, 201 (2003).
[86] S. D. Odintsov, V. K. Oikonomou, and P. V. Tretyakov, Phys. Rev. D **96**, 044022 (2017).
[87] S. D. Odintsov and V. K. Oikonomou, Phys. Rev. D **98**, 024013 (2018).
[88] S. Wiggins, S. Wiggins, and M. Golubitsky, *Introduction to Applied Nonlinear Dynamical Systems and Chaos* (Springer, New York, 2003), Vol. 2.
[89] B. Haasdonk, B. Hamzi, G. Santin, and D. Wittwar, Physica (Amsterdam) **427D**, 133007 (2021).
[90] J. Grzkedziński, J. Fluids Struct. **21**, 187 (2005).
[91] S. W. Hawking, Phys. Rev. D **13**, 191 (1976).
[92] T. Jacobson, Phys. Rev. Lett. **75**, 1260 (1995).
[93] R. Brustein, Phys. Rev. Lett. **84**, 2072 (2000).
[94] C. A. Egan and C. H. Lineweaver, Astrophys. J. **710**, 1825 (2010).
[95] H. M. Sadjadi, Phys. Rev. D **73**, 063525 (2006).
[96] J. de Freitas Pacheco and J. Horvath, Classical Quantum Gravity **24**, 5427 (2007).
[97] N. Mahata and S. Chakraborty, Mod. Phys. Lett. A **30**, 1550009 (2015).